

Article

Simulation of the Formation and Growth of Soot Aerosol Particles in a Premixed Combustion Process Using a Soot Aerosol Dynamics Model

Sung Hoon Park

Department of Environmental Engineering, Suncheon National University, Suncheon 57922, Korea; shpark@snu.ac.kr; Tel.: +82-61-750-3816

Abstract: Recently, an aerosol dynamics model—the Soot Aggregate Moment Model (SAMM)—that can efficiently trace the size distribution and morphology of soot particles was developed. In order to examine the applicability of SAMM in association with open-source CFD and combustion chemistry solvers, the formation and growth of soot particles in a premixed ethylene/air combustion were simulated by connecting SAMM with OpenSMOKE++ in this study. The simulation results were compared with available measurements and with the results of a previous study conducted using SAMM connected with an in-house CFD code and the CHEMKIN combustion chemistry package. Both CHEMKIN and OpenSMOKE++ underestimated C₂H₂ concentration compared to previous measurements, with deviation from the measured data being smaller for OpenSMOKE++. The chemical mechanism adopted in the CHEMKIN package was found to underestimate pyrene concentration by a factor of several tens. OpenSMOKE++ predicted much higher soot precursor concentrations than CHEMKIN, leading to a higher nucleation rate and a faster surface growth in the latter part of the reactor. This resulted in a reasonable soot production rate without introducing an artificial condensation enhancement factor. The overestimation of low-molecular-weight polycyclic aromatic hydrocarbons in the latter part of the reactor and the neglect of sintering led to an overprediction of soot production and primary particle number. This result indicates that accounting only for obliteration without sintering in SAMM could not simulate the merging of primary particles sufficiently. This indication merits further investigation.

Keywords: soot; carbon aerosol; aerosol dynamics; numerical modeling; combustion emission



Citation: Park, S.H. Simulation of the Formation and Growth of Soot Aerosol Particles in a Premixed Combustion Process Using a Soot Aerosol Dynamics Model. *Atmosphere* **2022**, *13*, 847. <https://doi.org/10.3390/atmos13050847>

Academic Editors: Chang H. Jung and Jiye Lee

Received: 25 April 2022

Accepted: 19 May 2022

Published: 23 May 2022

Publisher's Note: MDPI stays neutral with regard to jurisdictional claims in published maps and institutional affiliations.



Copyright: © 2022 by the author. Licensee MDPI, Basel, Switzerland. This article is an open access article distributed under the terms and conditions of the Creative Commons Attribution (CC BY) license (<https://creativecommons.org/licenses/by/4.0/>).

1. Introduction

The prediction of mass, size distribution, and morphology of soot aerosol particles emitted from combustion processes is crucial for the quantification of the effects of soot particles on air quality and climate [1–5]. Despite extensive experimental and numerical research outcomes during the past half-century, the soot formation mechanism remains unclear [5–7] because it is a complex process in which several physical and chemical phenomena, such as thermo-fluid dynamics [8–10], gas-phase and heterogeneous chemical reactions [11–14], and aerosol dynamics [15–17], are combined. A profound understanding of the soot formation mechanism requires a complicated investigation procedure including setting up mathematical models for these phenomena and verifying and revising them by comparing their predictions with measurements.

In the field of aerosol dynamics, the method of moments [18–20], the sectional method [4,21–24], and the stochastic approach [25–27] have widely been used. In particular, the method of moments is the most widely used for soot formation modeling because it has the highest computational efficiency. It poses the smallest computational burden to a computational fluid dynamics (CFD) model containing chemical reactions, which requires long computation time in itself. The most critical drawback of the method

of moments is that it often traces only values of several moments of soot particles, rather than explicit particle size distribution or aggregate morphology.

Recently, an aerosol dynamics model—the Fractal Aggregate Moment Model (FAMM)—was developed based on the method of moments to trace the characteristic bi-modal particle size distribution and morphology of fractal aggregate particles effectively [28]. Later, the FAMM was modified into the Soot Aerosol Moment Model (SAMM) [29] that could simulate the formation and growth of soot aerosol particles when it was combined with combustion chemistry packages such as CHEMKIN [30]. A comparison of the predictions of SAMM with available measurements showed that SAMM could predict the size distribution and morphology of soot particles more than 100 times faster than the sectional model and that the difference between the predictions of the two models was much smaller than the differences between the predictions and the measured data [29]. However, both models need to employ an artificial surface growth enhancement factor on top of the chemical mechanism used [31] for a reasonable agreement with the measured data. This result demonstrated that the largest uncertainty in the prediction of soot formation was associated with soot precursor production through gas-phase chemical reactions rather than with the subsequent aerosol dynamics. The prediction of soot formation in combustion flames requires the use of CFD models containing gas-phase chemistry mechanisms, which consume tremendous computation time owing to the large number of grids (reaching sometimes millions) needed for solving three-dimensional fluid dynamics equations [32]. In this regard, the employment of an efficient aerosol dynamics module, such as SAMM, is expected to be fruitful.

On the other hand, the use of open-source models is rapidly increasing in the field of CFD combustion modeling, where in-house codes [33,34] and commercial CFD models [35,36] have been used mostly. A representative example is the CFD software OpenFOAM [37,38] developed as an object-oriented C++ library package. With its strengths of being open-source and object-oriented, OpenFOAM has widely been used as a CFD framework for modeling various thermo-fluid phenomena including chemical reactions, such as laminar premixed flames [39,40], laminar diffusion flames [41,42], syngas combustion [43], and biomass pyrolysis [44]. OpenSMOKE++ [45] is also an object-oriented C++ library package for solving a set of differential equations in which combustion chemistry and thermodynamics are combined. Combined with the CFD software OpenFOAM, OpenSMOKE++ can be used to simulate combustion in laminar and turbulent flows [46,47].

In this study, in order to examine the applicability of the soot model SAMM in association with open-source CFD and combustion chemistry solvers, the formation and growth of soot aerosol particles was modeled by combining OpenSMOKE++ simulation with the aerosol dynamics simulation using SAMM. The model-predicted results were compared with available measurements as well as with previous SAMM simulation results obtained using the combination of an in-house CFD code and the CHEMKIN package.

2. Model Description

In this study, all simulations were conducted in two steps: (1) computation of gas phase combustion chemistry occurring in the reactor using OpenSMOKE++ and (2) soot chemistry and dynamics calculations using SAMM. In this section, OpenSMOKE++ and SAMM, the two models used in this study, are introduced briefly, and the model settings are explained.

2.1. OpenSMOKE++

OpenSMOKE++ is equipped with the gas-phase chemistry mechanism of Ranzi et al. [14] composed of about 200 species and 6300 chemical reactions and a soot module [48] that can simulate large polycyclic aromatic hydrocarbons (PAHs) with carbon atom number equal to or larger than 20 and aerosol particles using a sectional method. However, the soot module embedded in OpenSMOKE++ assumes rates of aerosol dynamics mechanisms, such as nucleation, condensation, and coagulation, to be constant,

irrespective of particle size. It also assumes that the soot particle morphology is simply either spherical up to a certain size or aggregated for larger particles. Therefore, in this study, OpenSMOKE++ was used only up to the production of PAHs. Subsequent aerosol dynamics leading to soot formation and growth were simulated using SAMM.

In the framework of OpenSMOKE++, high-molecular-weight (HMW) PAH molecules and soot particles are divided into several “BINs”. BIN1 is defined as having the average carbon atom number of 20. Subsequent BINs are defined by doubling the average carbon atom number successively. Although BIN1 to BIN4 are called HMW PAHs, and BIN5 and larger ones are called soot particles in OpenSMOKE++, this classification is quite arbitrary. In a previous study of the author using SAMM [29], soot inception (nucleation) was assumed to take place by collisions between two pyrene molecules with carbon atom number 16 (C16). Similarly, in this study, it was assumed that collisions between two BIN1 molecules caused nucleation. Surface growth due to condensation of vapor species was assumed to be caused by low-molecular-weight (LMW) PAHs that were smaller than BIN1 molecules. The concentrations of all species up to BIN1 simulated by OpenSMOKE++ based on its gas-phase chemistry were transferred to SAMM, in which aerosol dynamics were calculated to model soot formation and growth.

Nucleation and vapor condensation are gas-particle conversion mechanisms connecting gas-phase reactions and aerosol dynamics. Hence, they are closely associated with gas-phase mechanisms. Therefore, collision efficiency as an element employed in OpenSMOKE++ needed to be adopted in SAMM. When collision rates are calculated for nucleation (collision between PAH molecules) and condensation (collision between a soot particle and a PAH molecule) in OpenSMOKE++, the following collision efficiency, suggested based on the experiment of D’Alessio et al. [49], is multiplied:

$$\gamma = \frac{10^2 + \sigma^{6.5}}{10^5 + \sigma^{6.5}} \quad (1)$$

where σ is the collision diameter expressed in nm. Figure 1 shows this collision efficiency as a function of the collision diameter of soot particle. While the collision efficiency is 0.001 in the case of fresh nucleus particles with a diameter of about 1 nm or less, it increases with an increasing collision diameter until it reaches 1 for soot particles that grow larger than 10 nm at the latter part of the reactor. In the case of nucleation, the collision diameter, which is the diameter of BIN1 PAH molecules, is smaller than 1 nm. Thus, γ is always 0.001.

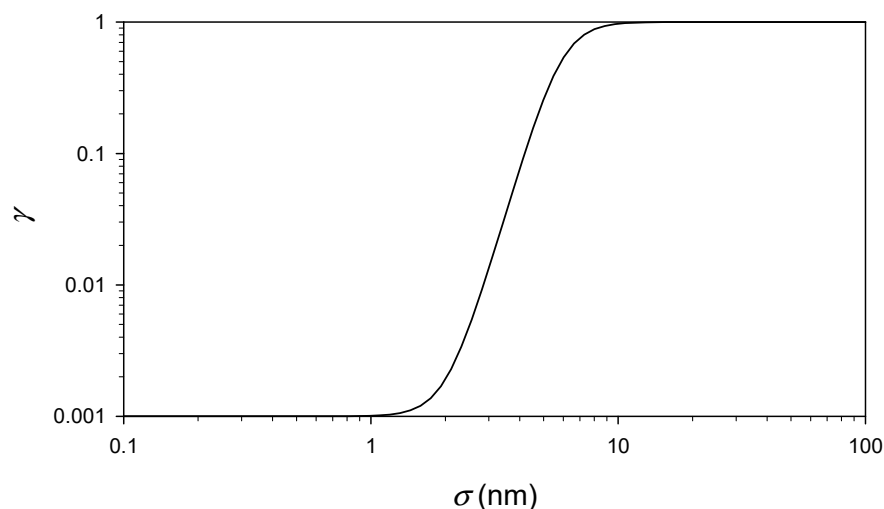


Figure 1. Collision efficiency as a function of the collision diameter of the soot particle.

The growth of soot particles due to surface reactions is represented by the well-known hydrogen abstraction–C₂H₂ addition (HACA) [50,51]. OpenSMOKE++ takes into account surface reactions of resonantly stabilized LMW radicals (C₃H₃, *i*-C₄H₃, *i*-C₄H₅, and C₅H₅) as well. Aromatic hydrocarbon radicals, including the radicals of single-ring aromatic hydrocarbons from benzene (C₆) to ethylbenzene (C₈) and PAH species from indene (C₉) to pyrene (C₁₆) are considered as the soot precursor species contributing to surface growth by condensation [48].

2.2. SAMM

SAMM includes the aerosol dynamics mechanisms necessary for simulating the changes in soot particle size distribution and morphology, such as nucleation, coagulation, PAH condensation, surface growth through heterogeneous reactions, obliteration of primary particles due to surface growth, and sintering. However, sintering was neglected in this study because of the lack of sufficient measured data for the sintering rate of soot particles [52]. Influences of the neglect of sintering will be discussed in Section 3 where model predictions are compared with measurements.

Since the structure and mathematical principles of SAMM have been presented in detail in a previous paper [29], only a brief explanation of its core elements is presented here. The main emphasis is on model revisions made for connecting with OpenSMOKE++.

SAMM assumes that soot aerosol particles attain a bimodal size distribution composed of a nuclei mode containing fresh particles generated by nucleation and an accumulation mode containing larger particles grown from nuclei-mode particles. Nuclei-mode particles are spherical and monodisperse, whereas accumulation-mode particles are aggregated and polydisperse, and their distribution can be expressed by a log-normal function. Therefore, nuclei-mode particles can be represented by a single variable (particle number), whereas accumulation-mode particles are represented by four variables (aggregate number, geometric mean aggregate size, geometric standard deviation of aggregate size, and primary particle number). Therefore, SAMM predicts size distribution and morphology of soot particles by tracing the time evolutions of these five variables. When nuclei-mode particles grow via coagulation, PAH condensation, and/or surface reaction, moving all grown particles into the accumulation mode may make the size distribution of the accumulation mode unrealistically broad. Therefore, appropriate schemes are used to apportion grown particles between nuclei and accumulation modes, so that total particle number and mass are conserved [28,53].

Nucleation, i.e., the production of new soot particles, is assumed to take place by collisions of PAH molecules that are large enough. For instance, in a previous study of the author [29], pyrene (C₁₆H₁₀) was selected as the precursor for nucleation. As explained in Section 2.1, HMW PAHs are represented by BIN1~BIN4 molecules in the chemistry solver OpenSMOKE++. As the average molecular mass of BIN1 molecules (250) is larger than that of pyrene (202), BIN1 molecules were selected as nucleation precursors in this study. Particles generated from collisions between the BIN1 molecules (i.e., BIN2 molecules in OpenSMOKE++) were regarded as soot nuclei. In SAMM, the collision rate between nucleation precursors (i.e., BIN1 molecules) is determined according to the free-molecule regime collision scheme based on the kinetic theory of gas [54]. Because the gas-phase chemistry of OpenSMOKE++ was used in this study up to precursor PAHs, the collision efficiency for nucleation used in OpenSMOKE++ ($\gamma = 0.001$) was applied in SAMM as well for fair comparison between the models.

In the original SAMM, six heterogeneous reactions including HACA and soot oxidation by OH and O₂ were taken into account for surface growth according to the mechanism suggested by Appel et al. [31]. For fair comparison with OpenSMOKE++, surface reactions of resonantly stabilized LMW radicals were added to SAMM in this study. However, the simulation results showed that the influences of LMW radicals on soot surface growth were negligible because their concentrations were much lower than the concentration of C₂H₂.

Pyrene was the only PAH species considered for condensation on the soot surface in the original SAMM based on the mechanism of Appel et al. [31]. However, various PAH species other than pyrene have been suggested as candidate contributors to soot growth by condensation [55,56], which could result in faster surface growth than that estimated by the mechanism of Appel et al. [31] considering only pyrene. In this study, SAMM was revised by allowing C9 (indene) and heavier LMW PAH molecules to be additional condensable species. The collision efficiency shown in Equation (1) was also employed when the rate of collision between a soot particle and a condensable species was calculated.

Coagulation is described in SAMM as aggregation without coalescence; individual coagulation events result in only a reduction of the total aggregate number by 1, without any changes in total primary particle number or total soot mass. Intramodal coagulations occurring in the nuclei or accumulation mode and intermodal coagulation occurring between the two modes are taken into account. In the case of intramodal coagulation in the nuclei mode, the resulting particles are apportioned between nuclei and accumulation modes, as mentioned above. A collision kernel calculated as the harmonic mean [57] of the free-molecule regime kernel [54] and the continuum-regime kernel [58] is used for the entire particle size range.

2.3. Numerical Experiments

A rich premixed ethylene/air combustion in a jet-stirred reactor (JSR)–plug flow reactor (PFR) system was simulated using OpenSMOKE++. Gas-phase species concentrations predicted by OpenSMOKE++ were used as input fields for aerosol dynamics simulation by SAMM. The model-predicted time evolutions of soot particle size distribution and morphology were compared with available measurements [59,60] as well as with previous SAMM simulation results obtained using an in-house CFD code and the CHEMKIN package. The present model system, in which OpenSMOKE++ and SAMM are combined, is referred to as “OpenSMOKE-SAMM”, whereas the previous one, in which the in-house CFD code, the CHEMKIN package, and SAMM were combined, is called “CHEMKIN-SAMM” hereafter. One can refer to the above-mentioned papers for detailed information on the measurement methods and to previous papers of the author [23,29] for detailed information on the setup for numerical simulations. The soot precursor species used for different gas-to-particle mechanisms in the two model systems are compared in Table 1.

Table 1. Soot precursor species for different gas-to-particle mechanisms.

Mechanism	CHEMKIN-SAMM	OpenSMOKE-SAMM
Nucleation	Pyrene	BIN1 molecules
Condensation	Pyrene	LMW PAHs (C9 to C16)
Surface reaction	C ₂ H ₂	C ₂ H ₂ , C ₃ H ₃ , <i>i</i> -C ₄ H ₃ , <i>i</i> -C ₄ H ₅ , and C ₅ H ₅

3. Results and Discussion

Figure 2 compares the concentration of a heterogeneous reaction precursor, C₂H₂, predicted by OpenSMOKE++ with measured data and that predicted previously by the CHEMKIN package. Both CHEMKIN and OpenSMOKE++ underpredicted C₂H₂ concentration compared to previous measurements, with the prediction of OpenSMOKE++ being slightly closer to the measurement.

Other than heterogeneous reactions, another mechanism that contributes to soot surface growth in SAMM is PAH condensation. PAHs are important soot precursors that contribute to soot production not only by condensation, but also by nucleation. The concentrations of PAHs predicted by the two models were compared with measurement data as shown in Figure 3. Marr et al. [59] analyzed LMW PAH species with molecular mass of 226 or smaller (C₁₂–C₁₈) using GC–FID, GC–MS, GC–FTIR, and HPLC. The amount of HMW PAHs with molecular mass larger than 226 was determined by subtracting LMW PAH mass from the total PAH mass determined gravimetrically. Because CHEMKIN-SAMM

considers only pyrene as the soot precursor contributing to nucleation and condensation (see Table 1), only the pyrene concentration predicted by CHEMKIN is included in Figure 3. On the other hand, OpenSMOKE-SAMM considers not only pyrene, but also other LMW PAHs for condensation. Therefore, the pyrene concentration as well as the LMW PAHs concentration predicted by OpenSMOKE++ are compared together in Figure 3. The concentration of “BIN1” molecules predicted by OpenSMOKE++ was also compared because BIN1 molecules represent most of the mass of HMW PAHs and are soot precursors for nucleation in OpenSMOKE-SAMM.

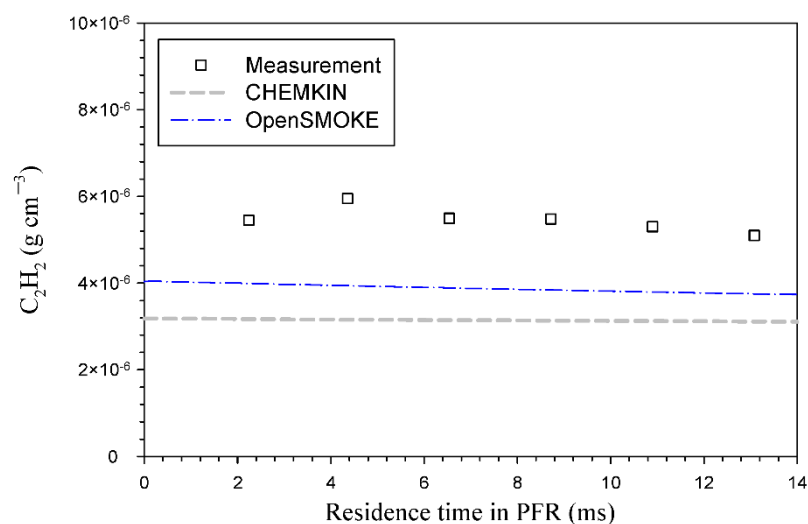


Figure 2. Comparison of C_2H_2 concentrations predicted by CHEMKIN and OpenSMOKE++ with measured C_2H_2 concentrations reported by Marr et al. [59].

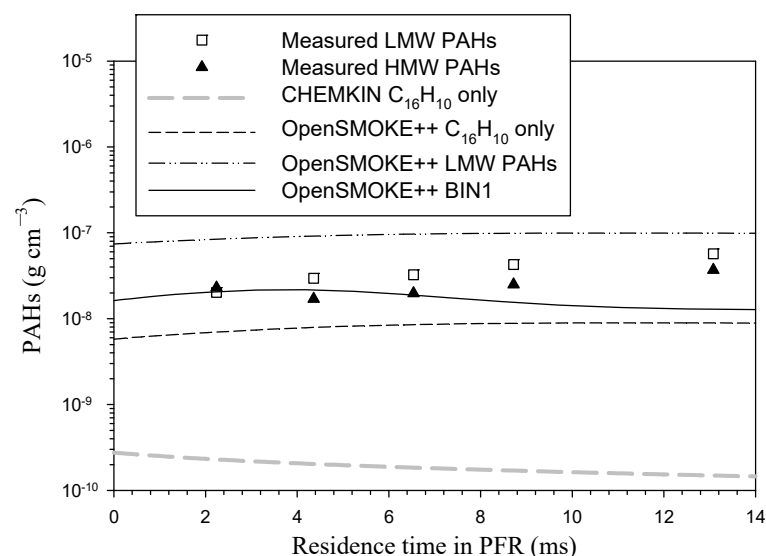


Figure 3. Comparison of PAH concentrations predicted by CHEMKIN and OpenSMOKE++ with measured data.

As shown in Figure 3, there was a striking difference (by a factor of several tens) between pyrene concentrations predicted by CHEMKIN and OpenSMOKE++. Considering that the LMW PAHs mass predicted by OpenSMOKE++ was in order-of-magnitude agreement with the measurement, it appeared that the mechanism of Appel et al. [31] used in CHEMKIN underestimated the production of pyrene considerably. In terms of nucleation, the mass concentration of BIN1 molecules predicted by OpenSMOKE++ was about 50 times higher than the pyrene mass concentration predicted by CHEMKIN. This indicated that the

difference between the square of number concentration to determine the nucleation rate was more than 1000 times even after converting it into number concentration. Therefore, even with a collision efficiency of 0.001, the nucleation rate predicted by OpenSMOKE-SAMM was larger than that predicted by CHEMKIN-SAMM. On the other hand, in terms of condensation, the LMW PAHs concentration predicted by OpenSMOKE++ was more than 100 times larger than the pyrene concentration predicted by CHEMKIN. This implies that the condensation rate predicted by OpenSMOKE-SAMM will be smaller than that predicted by CHEMKIN-SAMM in the initial stage of the combustion because of the very small soot particle size and, correspondingly, low collision efficiency (~ 0.001). However, as soot particles grow in the latter part of the reactor, the increase in collision efficiency (see Figure 1) will lead to a much larger condensation rate according to OpenSMOKE-SAMM than according to CHEMKIN-SAMM. This is shown below in Figure 4. Concentrations of LMW PAH and HMW PAH (represented by BIN1) predicted by OpenSMOKE++ showed overestimation and underestimation, respectively, compared to the measurements, resulting in comparable total PAH concentration.

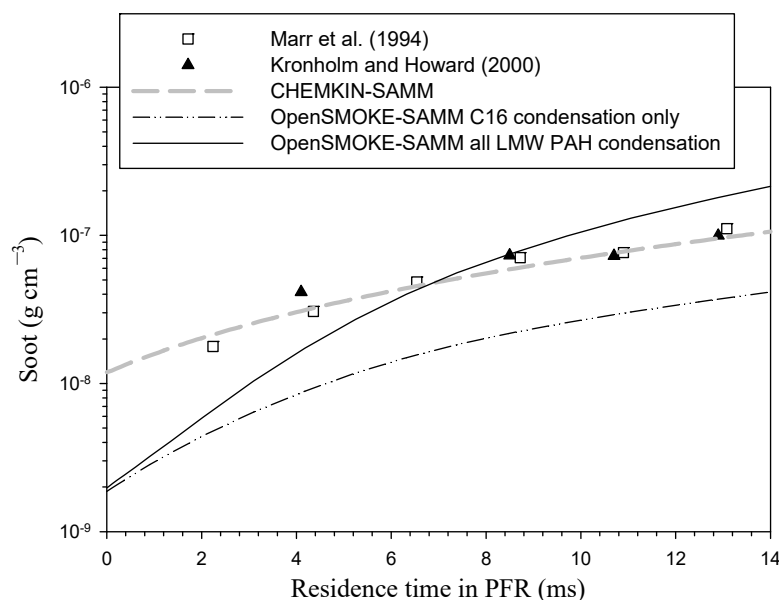


Figure 4. Comparison of soot mass concentrations predicted by CHEMKIN-SAMM and OpenSMOKE-SAMM with measured data [59,60].

Soot mass concentrations predicted by CHEMKIN-SAMM and OpenSMOKE-SAMM were compared with measured data of Marr et al. [59] and Kronholm and Howard [60] in Figure 4. Although OpenSMOKE-SAMM predicted higher concentrations for the two important soot precursors C_2H_2 and pyrene than CHEMKIN-SAMM (see Figures 2 and 3), it predicted lower soot mass concentration than CHEMKIN-SAMM when only pyrene was used as the precursor for condensation (pyrene condensation only). This has two reasons. The first reason is the collision efficiency of Equation (1) applied only to OpenSMOKE-SAMM when calculating the collision rate between a PAH molecule and a soot particle. As explained in the discussion for Figure 3, the collision efficiency is very small in the initial stage of a combustion reaction. The second reason is an artificial condensation enhancement factor adopted in CHEMKIN-SAMM to compensate for the neglect of other condensable species than pyrene [23,29]. When all LMW PAH species were used for condensation in OpenSMOKE-SAMM (all LMW PAH condensation), a much larger soot mass concentration, which was closer to the measurement, was predicted.

While the “all LMW PAH condensation” simulation of OpenSMOKE-SAMM shown in Figure 4 provided the best result using this model, its prediction still showed a large difference from the measurement; the soot mass was underpredicted considerably in the

early part of the reactor, whereas it was overpredicted significantly in the latter part of the reactor. This was because, as explained in the discussion for Figure 3, the condensation rate predicted by OpenSMOKE-SAMM was initially smaller than that predicted by CHEMKIN-SAMM but became larger than the latter as the soot particles grew. The overprediction of LMW PAH concentration by OpenSMOKE-SAMM shown in Figure 3 might have also contributed to the overprediction of soot mass in the latter part of the reactor. The neglect of sintering, which will be discussed later, is also a possible reason for soot mass overprediction in the latter part of the reactor.

Figure 5 shows soot particle size distributions predicted by CHEMKIN-SAMM and OpenSMOKE-SAMM as well as the measurements by Kronholm and Howard [60]. OpenSMOKE-SAMM predicted narrower particle size distributions than CHEMKIN-SAMM, which could be attributed to the higher surface growth rate of OpenSMOKE-SAMM, particularly in the latter part of the reactor, as mentioned earlier when discussing Figures 3 and 4. It is well known that a strong surface growth leads to a narrow particle size distribution [61]. Another notable difference between models' predictions was that the amount of nuclei-mode particles predicted by OpenSMOKE-SAMM was much larger than that predicted by CHEMKIN-SAMM. This could be attributed to a higher nucleation rate of OpenSMOKE-SAMM than of CHEMKIN-SAMM, as mentioned earlier when discussing Figure 3. Compared with the measured size distribution, OpenSMOKE-SAMM underpredicted the particle size at 4.2 ms, whereas it overpredicted the particle size at 12.9 ms, in agreement with the result for soot mass shown in Figure 4.

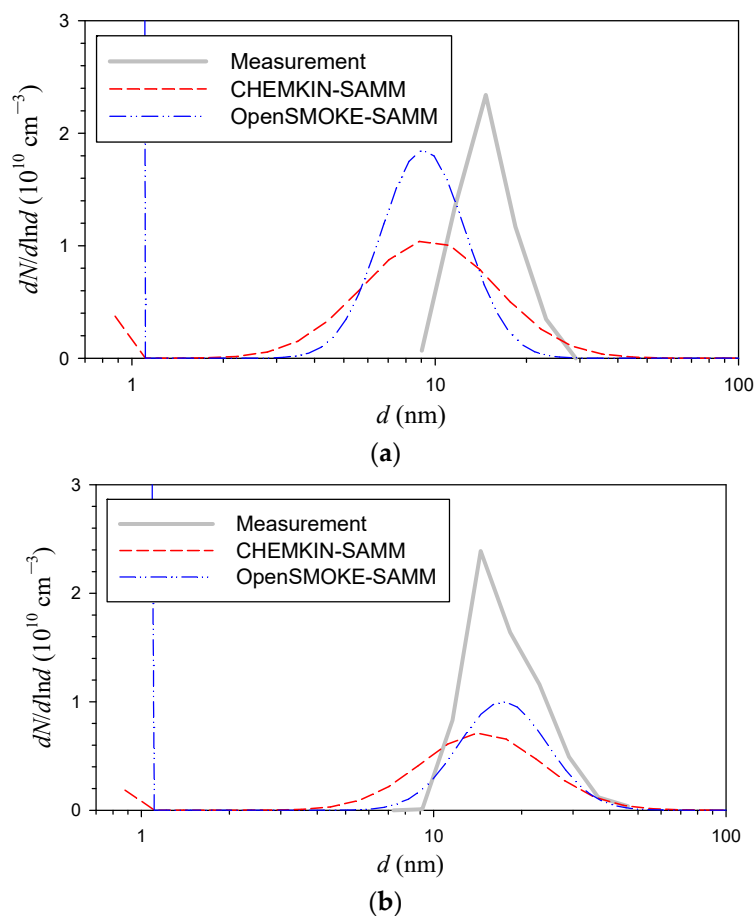


Figure 5. Cont.

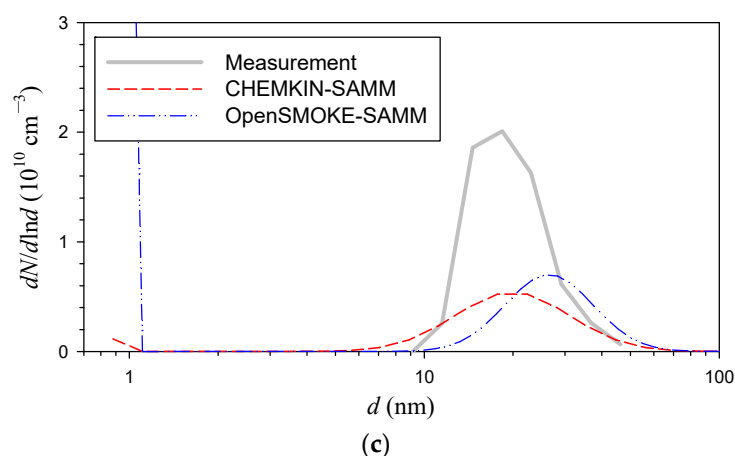


Figure 5. Comparison of soot particle size distributions predicted by CHEMKIN-SAMM and OpenSMOKE-SAMM with measured data at different residence times in the PFR: (a) 4.1 ms, (b) 8.5 ms, and (c) 12.9 ms.

In SAMM, the soot particles are assumed to be fractal aggregates consisting of spherical primary particles with a fractal dimension of 1.8. Therefore, the morphology of a soot aggregate particle can be determined once the number of primary particles composing it is known. In Figure 6, the average numbers of primary particles in a soot aggregate particle predicted by OpenSMOKE-SAMM and CHEMKIN-SAMM were compared. OpenSMOKE-SAMM predicted a smaller number of primary particles in an aggregate than CHEMKIN-SAMM in the earlier part of the reactor. In the latter part of the reactor, however, it predicted a larger number of primary particles than CHEMKIN-SAMM. This might be attributed to the higher nucleation rate predicted by OpenSMOKE-SAMM producing more nuclei, which might have been converted into aggregates by rapid coagulation in the latter part of the reactor.

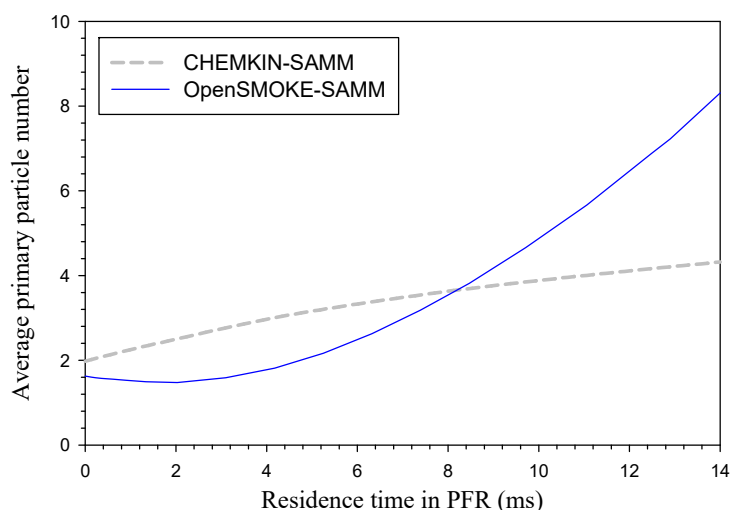


Figure 6. Comparison of the average primary particle number predicted by OpenSMOKE-SAMM and CHEMKIN-SAMM.

As mentioned above, SAMM treats coagulation as aggregation (without coalescence) in which the total number of primary particles does not change. Because combustion is a high-temperature process by nature, coagulation between fresh soot particles produced in combustion flames is often accompanied by fast sintering leading to spherical particles [62]. Therefore, the neglect of sintering in SAMM inevitably results in an overestimation of the primary particle number. Kronholm and Howard [60] reported that soot particles were

mostly spherical, including only a small amount of aggregate particles, in their experiments. In this respect, the predictions of both models shown in Figure 6 are obvious overestimations. An overestimation of the primary particle number will lead to an overestimation of the collision diameters of soot particles. This in turn will result in an overprediction of the surface growth rate, consequently leading to an overestimation of soot mass concentration. The overpredictions of soot mass concentration and particle size shown in Figures 4 and 5, respectively, by OpenSMOKE-SAMM in the latter part of the reactor were very likely to be influenced by the overestimation of primary particle number, at least in part.

The above-mentioned discussion indicates that obliteration of primary particles due to surface growth, which is accounted for in the current version of SAMM, is insufficient to model the merging of primary particles. Sintering might have to be taken into account for a more accurate simulation of soot particle mass, size, and morphology. This conclusion is quite different from those of previous studies [62–64], in which the effect of sintering was smaller than that of obliteration in the case of soot particles. Further investigations on this issue are warranted. As mentioned earlier, the current version of SAMM does not model sintering because of the lack of sufficient measurements of the sintering rate of soot particles [52]. However, a sufficiently accurate sintering model is expected to be available for SAMM in the near future thanks to active ongoing research studies on the sintering of soot particles [65–67]. Such model will enhance the applicability of SAMM further.

4. Conclusions

A combustion chemistry solver OpenSMOKE++ was connected with a recently developed soot aerosol dynamics code SAMM to simulate the formation and growth of soot aerosol particles in a premixed ethylene/air combustion. The simulation results were compared with results of a previous modeling study using an in-house CFD code and the CHEMKIN package as well as with available measurements. Both CHEMKIN and OpenSMOKE++ underpredicted C_2H_2 concentration compared to previous measurements. The gas-phase chemistry used in CHEMKIN underpredicted the production of pyrene severely, which resulted in an underestimated nucleation rate. OpenSMOKE++ predicted a much higher LMW PAHs concentration than CHEMKIN, enabling the soot surface growth rate to be simulated reasonably without an artificial condensation enhancement factor. In the latter part of the reactor, the LMW PAHs concentration was even overestimated by OpenSMOKE++, which (in addition to the effect of the neglect of sintering) led to overestimating soot growth rate and primary particle number. The results of this study demonstrate that OpenSMOKE++ is a promising tool for modeling soot production if it is combined with an elaborate aerosol dynamics model. However, this study also revealed the limitations of the current version of SAMM. The effect of obliteration was shown not to be large enough to account for the observed primary particles merging with neglected sintering. This was different from results of previous studies reporting that the effect of sintering was less important than that of obliteration. This requests further investigation and appropriate model revisions to reduce uncertainties. If the results of recent studies on the sintering rate of soot particles are utilized properly, the applicability of SAMM is expected to be further enhanced.

Funding: This research was supported by the Basic Science Research Program through the National Research Foundation of Korea (NRF) funded by the Ministry of Education (2019R1D1A3A03103860).

Data Availability Statement: Not applicable.

Acknowledgments: The author thanks Alberto Cuoci at Politecnico di Milano for providing the OpenSMOKE++ Suite.

Conflicts of Interest: The author declares no conflict of interest.

References

1. Donaldson, K.; Tran, L.; Jimenez, L.A.; Duffin, R.; Newby, D.E.; Mills, N.; MacNee, W.; Stone, V. Combustion-derived nanoparticles: A review of their toxicology following inhalation exposure. *Part. Fibre Toxicol.* **2005**, *2*, 10. [[CrossRef](#)]
2. Park, S.H.; Gong, S.L.; Bouchet, V.S.; Gong, W.; Makar, P.A.; Moran, M.D.; Stroud, C.A.; Zhang, J. Effects of black carbon aging on air quality predictions and direct radiative forcing estimation. *Tellus B* **2011**, *63*, 1026–1039. [[CrossRef](#)]
3. Zhang, R.; Kook, S. Influence of fuel injection timing and pressure on in-flame soot particles in an automotive-size diesel engine. *Environ. Sci. Technol.* **2014**, *48*, 8243–8250. [[CrossRef](#)]
4. Aubagnac-Karkar, D.; Michel, J.; Colin, O.; Vervisch-Kljakic, P.E.; Darabiha, N. Sectional soot model coupled to tabulated chemistry for Diesel RANS simulations. *Combust. Flame* **2015**, *162*, 3081–3099. [[CrossRef](#)]
5. Michelsen, H.A. Probing soot formation, chemical and physical evolution, and oxidation: A review of in situ diagnostic techniques and needs. *Proc. Combust. Inst.* **2017**, *36*, 717–735. [[CrossRef](#)]
6. Wang, H. Formation of nascent soot and other condensed-phase materials in flames. *Proc. Combust. Inst.* **2011**, *33*, 41–67. [[CrossRef](#)]
7. Zhao, F.; Yang, W.; Yu, W. A progress review of practical soot modelling development in diesel engine combustion. *J. Traffic Transp. Eng.* **2020**, *7*, 269–281. [[CrossRef](#)]
8. Wang, L.; Haworth, D.C.; Turns, S.R.; Modest, M.F. Interactions among soot, thermal radiation, and NO_x emissions in oxygen-enriched turbulent nonpremixed flames: A computational fluid dynamics modeling study. *Combust. Flame* **2005**, *141*, 170–179. [[CrossRef](#)]
9. Lucchini, T.; D’Errico, G.; Onorati, A.; Bonandrini, G.; Venturoli, L.; Di Gioia, R. Development and application of a computational fluid dynamics methodology to predict fuel–air mixing and sources of soot formation in gasoline direct injection engines. *Int. J. Engine Res.* **2014**, *15*, 581–596. [[CrossRef](#)]
10. Tan, J.Y.; Bonatesta, F.; Ng, H.K.; Gan, S. Developments in computational fluid dynamics modelling of gasoline direct injection engine combustion and soot emission with chemical kinetic modelling. *Appl. Therm. Eng.* **2016**, *107*, 936–959. [[CrossRef](#)]
11. Lu, T.; Law, C.K. Toward accommodating realistic fuel chemistry in large-scale computations. *Prog. Energy Combust. Sci.* **2009**, *35*, 192–215. [[CrossRef](#)]
12. Westbrook, C.K.; Pitz, W.J.; Herbinet, O.; Curran, H.J.; Silke, E.J. A comprehensive detailed chemical kinetic reaction mechanism for combustion of n-alkane hydrocarbons from n-octane to n-hexadecane. *Combust. Flame* **2009**, *156*, 181–199. [[CrossRef](#)]
13. Westbrook, C.K.; Naik, C.V.; Herbinet, O.; Pitz, W.J.; Mehl, M.; Sarathy, S.M.; Curran, H.J. Detailed chemical kinetic reaction mechanisms for soy and rapeseed biodiesel fuels. *Combust. Flame* **2011**, *158*, 742–755. [[CrossRef](#)]
14. Ranzi, E.L.I.S.E.O.; Frassoldati, A.; Grana, R.; Cuoci, A.; Faravelli, T.; Kelley, A.P.; Law, C.K. Hierarchical and comparative kinetic modeling of laminar flame speeds of hydrocarbon and oxygenated fuels. *Prog. Energy Combust. Sci.* **2012**, *38*, 468–501. [[CrossRef](#)]
15. Zhang, Q.; Guo, H.; Liu, F.; Smallwood, G.J.; Thomson, M.J. Implementation of an advanced fixed sectional aerosol dynamics model with soot aggregate formation in a laminar methane/air coflow diffusion flame. *Combust. Theory Model.* **2008**, *12*, 621–641. [[CrossRef](#)]
16. Roy, S.P.; Arias, P.G.; Lecoustre, V.R.; Haworth, D.C.; Im, H.G.; Trouvé, A. Development of high fidelity soot aerosol dynamics models using method of moments with interpolative closure. *Aerosol Sci. Technol.* **2014**, *48*, 379–391. [[CrossRef](#)]
17. Rigopoulos, S. Modelling of soot aerosol dynamics in turbulent flow. *Flow Turbul. Combust.* **2019**, *103*, 565–604. [[CrossRef](#)]
18. Frenklach, M.; Wang, H. Detailed mechanism and modeling of soot particle formation. In *Soot Formation in Combustion: Mechanisms and Models*; Bockhorn, H., Ed.; Springer: Berlin/Heidelberg, Germany, 1994; pp. 165–192.
19. Wick, A.; Nguyen, T.; Laurent, F.; Fox, R.O.; Pitsch, H. Modeling soot oxidation with the Extended Quadrature Method of Moments. *Proc. Combust. Inst.* **2017**, *36*, 789–797. [[CrossRef](#)]
20. Salenbauch, S.; Hasse, C.; Vanni, M.; Marchisio, D.L. A numerically robust method of moments with number density function reconstruction and its application to soot formation, growth and oxidation. *J. Aerosol Sci.* **2019**, *128*, 34–49. [[CrossRef](#)]
21. Colket, M.B.; Hall, R.J. Successes and uncertainties in modeling soot formation in laminar, premixed flames. In *Soot formation in Combustion: Mechanisms and Models*; Bockhorn, H., Ed.; Springer: Berlin, Germany, 1994; pp. 442–470.
22. Pope, C.J.; Howard, J.B. Simultaneous particle and molecule modeling (SPAMM): An approach for combining sectional aerosol equations and elementary gas-phase reactions. *Aerosol Sci. Technol.* **1997**, *27*, 73–94. [[CrossRef](#)]
23. Park, S.H.; Rogak, S.N.; Bushe, W.K.; Wen, J.Z.; Thomson, M.J. An aerosol model to predict size and structure of soot particles. *Combust. Theory Model.* **2005**, *9*, 499–513. [[CrossRef](#)]
24. Blacha, T.; Di Domenico, M.; Gerlinger, P.; Aigner, M. Soot predictions in premixed and non-premixed laminar flames using a sectional approach for PAHs and soot. *Combust. Flame* **2012**, *159*, 181–193. [[CrossRef](#)]
25. Goodson, M.; Kraft, M. An efficient stochastic algorithm for simulating nano-particle dynamics. *J. Comput. Phys.* **2002**, *183*, 210–232. [[CrossRef](#)]
26. Balthasar, M.; Kraft, M. A stochastic approach to calculate the particle size distribution function of soot particles in laminar premixed flames. *Combust. Flame* **2003**, *133*, 289–298. [[CrossRef](#)]
27. Singh, J.; Balthasar, M.; Kraft, M.; Wagner, W. Stochastic modeling of soot particle size and age distributions in laminar premixed flames. *Proc. Combust. Inst.* **2005**, *30*, 1457–1465. [[CrossRef](#)]
28. Kim, M.Y.; Park, S.H. A numerical aerosol model Fractal Aggregate Moment Model (FAMM) to simulate simultaneous nucleation, coagulation, surface growth, and sintering of fractal aggregates. *Aerosol Sci. Technol.* **2019**, *53*, 493–507. [[CrossRef](#)]

29. Park, S.H. Bi-modal moment model for predicting the formation and growth of soot aggregate particles. *Particul. Sci. Technol.* **2022**. [[CrossRef](#)]
30. Kee, R.J.; Rupley, F.M.; Miller, J.A. *Chemkin-II: A Fortran Chemical Kinetics Package for the Analysis of Gas-Phase Chemical Kinetics*; Sandia National Lab. (SNL-CA): Livermore, CA, USA, 1989; Report No.: SAND-89-8009.
31. Appel, J.; Bockhorn, H.; Frenklach, M. Kinetic modeling of soot formation with detailed chemistry and physics: Laminar premixed flames of C2 hydrocarbons. *Combust. Flame* **2000**, *121*, 122–136. [[CrossRef](#)]
32. Eberle, C.; Gerlinger, P.; Geigle, K.P.; Aigner, M. Numerical investigation of transient soot evolution processes in an aero-engine model combustor. *Combust. Sci. Technol.* **2015**, *187*, 1841–1866. [[CrossRef](#)]
33. Yuen, A.C.Y.; Yeoh, G.H.; Timchenko, V.; Cheung, S.C.P.; Barber, T.J. Importance of detailed chemical kinetics on combustion and soot modelling of ventilated and under-ventilated fires in compartment. *Int. J. Heat Mass Transfer.* **2016**, *96*, 171–188. [[CrossRef](#)]
34. Akridis, P.; Rigopoulos, S. Modelling of soot formation in laminar diffusion flames using a comprehensive CFD-PBE model with detailed gas-phase chemistry. *Combust. Theory Model.* **2017**, *21*, 35–48. [[CrossRef](#)]
35. Balthasar, M.; Mauss, F.; Pfitzner, M.; Mack, A. Implementation and validation of a new soot model and application to aeroengine combustors. *J. Eng. Gas Turbines Power* **2002**, *124*, 66–74. [[CrossRef](#)]
36. Zucca, A.; Marchisio, D.L.; Barresi, A.A.; Fox, R.O. Implementation of the population balance equation in CFD codes for modelling soot formation in turbulent flames. *Chem. Eng. Sci.* **2006**, *61*, 87–95. [[CrossRef](#)]
37. Weller, H.G.; Tabor, G.; Jasak, H.; Fureby, C. A tensorial approach to computational continuum mechanics using object-oriented techniques. *Comput. Phys.* **1998**, *12*, 620–631. [[CrossRef](#)]
38. Jasak, H.; Jemcov, A.; Tukovic, Z. OpenFOAM: A C++ library for complex physics simulations. In *International Workshop on Coupled Methods in Numerical Dynamics*; IUC Dubrovnik Croatia: Dubrovnik, Croatia, 2007.
39. Atoof, H.; Emami, M.D. Numerical simulation of laminar premixed CH₄/air flame by flamelet-generated manifolds: A sensitivity analysis on the effects of progress variables. *J. Taiwan Inst. Chem. Eng.* **2016**, *60*, 287–293. [[CrossRef](#)]
40. Jiang, X.; Chan, T.L. Lagrangian particle tracking with new weighted fraction Monte Carlo method for studying the soot particle size distributions in premixed flames. *Int. J. Numer. Methods Heat Fluid Flow* **2022**, *32*, 1961–1998. [[CrossRef](#)]
41. Dworkin, S.B.; Zhang, Q.; Thomson, M.J.; Slavinskaya, N.A.; Riedel, U. Application of an enhanced PAH growth model to soot formation in a laminar coflow ethylene/air diffusion flame. *Combust. Flame* **2011**, *158*, 1682–1695. [[CrossRef](#)]
42. Messig, D.; Hunger, F.; Keller, J.; Hasse, C. Evaluation of radiation modeling approaches for non-premixed flamelets considering a laminar methane air flame. *Combust. Flame* **2013**, *160*, 251–264. [[CrossRef](#)]
43. Marzouk, O.A.; Huckaby, E.D. A comparative study of eight finite-rate chemistry kinetics for CO/H₂ combustion. *Eng. Appl. Comput. Fluid Mech.* **2010**, *4*, 331–356.
44. Gentile, G.; Cuoci, A.; Frassoldati, A.; Faravelli, T.; Ranzi, E. A comprehensive CFD model for the biomass pyrolysis. *Chem. Eng. Trans.* **2015**, *43*, 445–450. [[CrossRef](#)]
45. Cuoci, A.; Frassoldati, A.; Faravelli, T.; Ranzi, E. OpenSMOKE++: An object-oriented framework for the numerical modeling of reactive systems with detailed kinetic mechanisms. *Comput. Phys. Commun.* **2015**, *192*, 237–264. [[CrossRef](#)]
46. Cuoci, A.; Frassoldati, A.; Faravelli, T.; Ranzi, E. A computational tool for the detailed kinetic modeling of laminar flames: Application to C₂H₄/CH₄ coflow flames. *Combust. Flame* **2013**, *160*, 870–886. [[CrossRef](#)]
47. Li, Z.; Malik, M.R.; Cuoci, A.; Parente, A. Edcsmoke: A new combustion solver for stiff chemistry based on OpenFOAM[®]. In *AIP Conference Proceedings*; AIP Publishing LLC: Melville, NY, USA, 2017.
48. Saggese, C.; Ferrario, S.; Camacho, J.; Cuoci, A.; Frassoldati, A.; Ranzi, E.; Wang, H.; Faravelli, T. Kinetic modeling of particle size distribution of soot in a premixed burner-stabilized stagnation ethylene flame. *Combust. Flame* **2015**, *162*, 3356–3369. [[CrossRef](#)]
49. D’Alessio, A.; Barone, A.C.; Cau, R.; D’Anna, A.; Minutolo, P. Surface deposition and coagulation efficiency of combustion generated nanoparticles in the size range from 1 to 10 nm. *Proc. Combust. Inst.* **2005**, *30*, 2595–2603. [[CrossRef](#)]
50. Frenklach, M.; Wang, H. Detailed modeling of soot particle nucleation and growth. In *Symposium (International) on Combustion*; Elsevier: Amsterdam, The Netherlands, 1991.
51. Frenklach, M. Reaction mechanism of soot formation in flames. *Phys. Chem. Chem. Phys.* **2002**, *4*, 2028–2037. [[CrossRef](#)]
52. Chen, D.; Zainuddin, Z.; Yapp, E.; Akroyd, J.; Mosbach, S.; Kraft, M. A fully coupled simulation of PAH and soot growth with a population balance model. *Proc. Combust. Inst.* **2013**, *34*, 1827–1835. [[CrossRef](#)]
53. Jeong, J.I.; Choi, M. A simple bimodal model for the evolution of non-spherical particles undergoing nucleation, coagulation and coalescence. *J. Aerosol Sci.* **2003**, *34*, 965–976. [[CrossRef](#)]
54. Matsoukas, T.; Friedlander, S.K. Dynamics of aerosol agglomerate formation. *J. Colloid Interface Sci.* **1991**, *146*, 495–506. [[CrossRef](#)]
55. Zhang, H.R.; Violi, A.; Sarofim, A.F.; Frenklach, M. A simulation of soot formation using particle dynamics with one dimensional nucleation mode. In *Proceedings of the Third Joint Meeting of the US Sections of the Combustion Institute, The central States Section, Chicago, IL, USA, 16–19 March 2003*.
56. Wen, J.Z.; Thomson, M.J.; Park, S.H.; Rogak, S.N.; Lightstone, M.F. Study of soot growth in a plug flow reactor using a moving sectional model. *Proc. Combust. Inst.* **2005**, *30*, 1477–1484. [[CrossRef](#)]
57. Pratsinis, S.E. Simultaneous nucleation, condensation, and coagulation in aerosol reactors. *J. Colloid Interface Sci.* **1988**, *124*, 416–427. [[CrossRef](#)]
58. Rogak, S.N.; Flagan, R.C. Coagulation of aerosol agglomerates in the transition regime. *J. Colloid Interface Sci.* **1992**, *151*, 203–224. [[CrossRef](#)]

59. Marr, J.A.; Giovane, L.M.; Longwell, J.P.; Howard, J.B.; Lafleur, A.L. Soot and tar production in a jet-stirred/plug-flow reactor system: High and low C₂H₂ concentration environments. *Combust. Sci. Technol.* **1994**, *101*, 301–309. [[CrossRef](#)]
60. Kronholm, D.F.; Howard, J.B. Analysis of soot surface growth pathways using published plug-flow reactor data with new particle size distribution measurements and published premixed flame data. *Proc. Combust. Inst.* **2000**, *28*, 2555–2561. [[CrossRef](#)]
61. Seinfeld, J.H.; Pandis, S.N. *Atmospheric Chemistry and Physics: From Air Pollution to Climate Change*, 3rd ed.; John Wiley & Sons: Hoboken, NJ, USA, 2016.
62. Kelesidis, G.A.; Goudele, E.; Pratsinis, S.E. Flame synthesis of functional nanostructured materials and devices: Surface growth and aggregation. *Proc. Combust. Inst.* **2017**, *36*, 29–50. [[CrossRef](#)]
63. Balthasar, M.; Frenklach, M. Detailed kinetic modeling of soot aggregate formation in laminar premixed flames. *Combust. Flame* **2005**, *140*, 130–145. [[CrossRef](#)]
64. Morgan, N.; Kraft, M.; Balthasar, M.; Wong, D.; Frenklach, M.; Mitchell, P. Numerical simulations of soot aggregation in premixed laminar flames. *Proc. Combust. Inst.* **2007**, *31*, 693–700. [[CrossRef](#)]
65. Veshkini, A.; Dworkin, S.B.; Thomson, M.J. Understanding soot particle size evolution in laminar ethylene/air diffusion flames using novel soot coalescence models. *Combust. Theory Model.* **2016**, *20*, 707–734. [[CrossRef](#)]
66. Ono, K.; Dewa, K.; Matsukawa, Y.; Saito, Y.; Matsushita, Y.; Aoki, H.; Era, K.; Aoki, T.; Yamaguchi, T. Experimental evidence for the sintering of primary soot particles. *J. Aerosol Sci.* **2017**, *105*, 1–9. [[CrossRef](#)]
67. Botero, M.L.; Eaves, N.; Dreyer, J.A.; Sheng, Y.; Akroyd, J.; Yang, W.; Kraft, M. Experimental and numerical study of the evolution of soot primary particles in a diffusion flame. *Proc. Combust. Inst.* **2019**, *37*, 2047–2055. [[CrossRef](#)]